Adaptive Lyapunov-constrained MPC for fault-tolerant AUV trajectory tracking

Haolin Liu, Shiliang Zhang, Xiaohui Zhang, Shangbin Jiao*, Xuehui Ma, Ting Shang, Yan Yan, Wenqi Bai, Youmin Zhang

Abstract—**Autonomous underwater vehicles (AUVs) are subject to various sources of faults during their missions, which challenges AUV control and operation in real environments. This paper addresses fault-tolerant trajectory tracking of autonomous underwater vehicles (AUVs) under thruster failures. We propose an adaptive Lyapunov-constrained model predictive control (LMPC) that guarantees stable trajectory tracking when the AUV switches between fault and normal modes. Particularly, we model different AUV thruster faults and build online failure identification based on Bayesian approach. This facilitates a soft switch between AUV status, and the identified and updated AUV failure model feeds LMPC controller for the control law derivation. The Lyapunov constrain in LMPC ensures that the trajectory tracking control remains stable during AUV status shifts, thus mitigating severe and fatal fluctuations when an AUV thruster occurs or recovers. We conduct numerical simulations on a four-thruster planar AUV using the proposed approach. The results demonstrate smooth transitions between thruster failure types and low trajectory tracking errors compared with the benchmark adaptive MPC and backstepping control with rapid failure identification and failure accommodation during the trajectory tracking.**

Index Terms—**Autonomous underwater vehicle (AUV), fault-tolerant control (FTC), Adaptive Lyapunov-Constrained MPC (ALMPC), Lyapunov-Constrained MPC (LMPC), Interacting Multiple Model (IMM), soft switching.**

I. Introduction

AUTONOMOUS underwater vehicles (AUVs) enable ocean observation, inspection, and intervention [1]–[4]. Among AUV propulsion solutions, propeller thrusters dominate practical platforms because of its advantages in efficiency and robustness [5], [6]. Reliable trajectory tracking in missions is a core capability for thrusters [7], [8]. In field operations, the control of thruster is subject to faults that arise from blockage or entanglement, blade breakage, mechanical looseness, and motor or gear failures [9], [10]. Reported statistics indicate that thrusters account for the majority of actuator faults in AUVs [9], [11]. Such faults can degrade tracking accuracy and and lead to failed missions and economic loss [12]. Therefore, the control of thrusters under fault conditions, a.k.a. fault-tolerant control, is of critical importance particularly in real world AUV missions.

The objective of fault-tolerant control (FTC) is to maintain stability and tracking accuracy under loss of effectiveness (LOE) and misalignment while respecting physical constraints. Recent FTC studies span passive and active schemes, diagnosis-aware reconfiguration, and robust or adaptive control [9], [13]–[15]. Multiple-model (MM) FTC has gained traction because it encodes a library of failure scenarios and coordinates controllers accordingly. However, many MM strategies rely on hard switching. Classical MM adaptive control and supervisory switching theory show that hard switching can induce transients unless hysteresis or dwell-time logic is enforced [16], [17]. With tight actuator limits and strong hydrodynamic couplings, these transients are often pronounced at fault instants, which motivates *soft switching* based on probability-weighted blending rather than winner-take-all selection [9], [18].

Within the controller bank, baseline laws (e.g. PID, LQR, Backstepping Control(BSC) and Sliding Mode Control(SMC)) remain attractive for simplicity and guaranteed basic performance [19]–[21]. Model predictive control (MPC) [22], [23] is increasingly preferred in modern banks because it handles constraints and can integrate thrust allocation in a receding-horizon optimization [24]. For nonlinear AUV dynamics, a finite-horizon MPC does not guarantee closed-loop stability or recursive feasibility without terminal ingredients. Lyapunov-based MPC (LMPC) addresses this gap by enforcing a *first-step Lyapunov contraction* derived from a stabilizing backstepping law. This yields stability under hard constraints and an integrated formulation with thrust allocation. LMPC has been demonstrated for dynamic positioning and trajectory tracking, with distributed and robust extensions [14], [25]–[29]. In severe LOE or misalignment, however, the quadratic objective must trade off state accuracy against control effort. If the prediction model does not reflect degraded actuation, practical MPC implementations may reduce effective actuation prematurely. To mitigate this, we introduce an *augmented-state LMPC*: slow force/torque biases and per-thruster LOE/misalignment parameters are estimated online as pseudo-states so that the prediction model and the allocation map track the prevailing fault [28]–[30].

On the inference side, we compute mode probabilities from innovation likelihoods using an Interacting Multiple
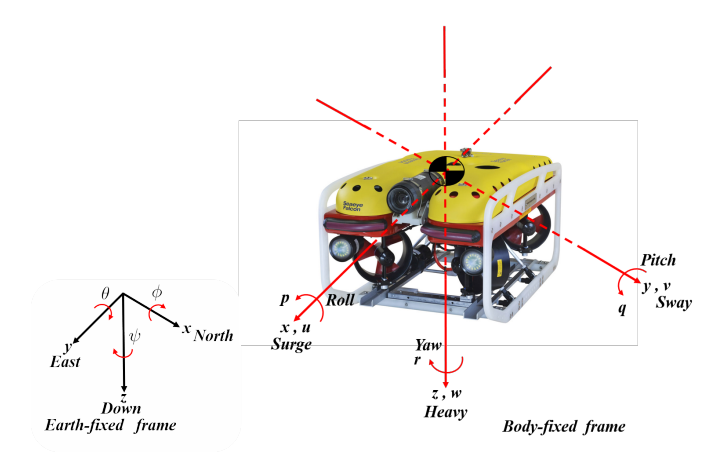
Fig. 1. Earth-fixed and body-fixed frames used for the Saab Seaeye Falcon.

Model (IMM) Bayesian recursion for Markovian switching systems [31]. The IMM update provides a principled and recursive mechanism to fuse evidence from a bank of mode-conditioned estimators. The resulting *posterior probabilities* schedule the controller bank via maximum-a-posteriori (MAP) selection or *probability-weighted blending* of mode-conditioned LMPC commands, followed by projection onto the admissible input set. This soft-fusion strategy preserves the per-mode LMPC contraction and mitigates switching transients relative to hard switching [16], [17], [32], [33].

Contributions. We propose an *adaptive Lyapunov-Constrained MPC (ALMPC)* architecture with three elements: (i) a bank of mode-conditioned LMPCs sharing a first-step Lyapunov contraction; (ii) a bias-augmented prediction model that estimates slow force/torque biases and per-thruster loss-of-effectiveness/misalignment online; (iii) an IMM-style Bayesian posterior that drives probability-weighted fusion with input projection. On a four-thruster planar AUV with nominal and two fault modes, ALMPC achieves smoother transitions and lower tracking error than Adaptive MPC(AMPC) and BSC while respecting input amplitude and rate limits.

Organization. Section II presents the AUV model, thrust mapping, and the augmented error model. Section III develops the ALMPC design. Section IV describes the Bayesian multi-model framework and control fusion. Section V reports simulations and comparisons. Section VI concludes.

II. PRELIMINARIES AND PROBLEM FORMULATION

This section introduces the 3-DOF kinematics and dynamics of the Saab Seaeye Falcon AUV and formulates the augmented error model used by the controller. Owing to its thruster configuration, the vehicle is underactuated in roll and pitch; thus we restrict attention to horizontal-plane motion and trajectory tracking in the Earth-fixed frame, see Fig 1.

A. AUV Kinematics and Dynamics

The planar kinematics are

$$\dot{\boldsymbol{\eta}} = \boldsymbol{J}(\psi)\,\boldsymbol{\nu}, \tag{1}$$

where $\boldsymbol{\eta} = [x, y, \psi]^\top$ is the Earth-fixed position and heading, $\boldsymbol{\nu} = [u, v, r]^\top$ is the body-fixed velocity, and

$$\boldsymbol{J}(\psi) = \begin{bmatrix} \cos\psi & -\sin\psi & 0 \\ \sin\psi & \cos\psi & 0 \\ 0 & 0 & 1 \end{bmatrix} = \begin{bmatrix} \boldsymbol{R}(\psi) & \boldsymbol{0} \\ 0 & 1 \end{bmatrix}. \tag{2}$$

The 3-DOF Newton–Euler dynamics in the body frame are

$$\boldsymbol{M}\,\dot{\boldsymbol{\nu}} + \boldsymbol{C}(\boldsymbol{\nu})\boldsymbol{\nu} + \boldsymbol{D}(\boldsymbol{\nu})\boldsymbol{\nu} = \boldsymbol{\tau} + \boldsymbol{w}, \tag{3}$$

where $\boldsymbol{M} = \boldsymbol{M}^\top \succ 0$ is the inertia matrix (including added mass), $\boldsymbol{C}(\boldsymbol{\nu}) = -\boldsymbol{C}^\top(\boldsymbol{\nu})$ is the Coriolis–centripetal matrix, $\boldsymbol{D}(\boldsymbol{\nu}) \succ 0$ is the hydrodynamic damping, $\boldsymbol{\tau} = [F_u, F_v, F_r]^\top$ is the generalized force/moment, and $\boldsymbol{w}$ collects bounded external disturbances.

Define the full state $\boldsymbol{x} = [\boldsymbol{\eta}^\top, \boldsymbol{\nu}^\top]^\top$. The state-space form follows from (1)–(3):

$$\dot{\boldsymbol{x}} = \begin{bmatrix} \boldsymbol{J}(\psi)\boldsymbol{\nu} \\ \boldsymbol{M}^{-1}(\boldsymbol{\tau} - \boldsymbol{C}(\boldsymbol{\nu})\boldsymbol{\nu} - \boldsymbol{D}(\boldsymbol{\nu})\boldsymbol{\nu}) \end{bmatrix} = \boldsymbol{f}(\boldsymbol{x}, \boldsymbol{\tau}). \tag{4}$$

B. Thruster Mapping and Fault Parameterization

The generalized force is produced by four thrusters via the allocation model

$$\boldsymbol{\tau} = \boldsymbol{T}(\boldsymbol{\theta})\,\boldsymbol{\Gamma}\,\boldsymbol{u}, \tag{5}$$

where $\boldsymbol{u} \in \mathbb{R}^{4 \times 1}$ stacks the individual thruster commands, $\boldsymbol{T}(\boldsymbol{\theta}) = [\boldsymbol{t}_1\ \boldsymbol{t}_2\ \boldsymbol{t}_3\ \boldsymbol{t}_4] \in \mathbb{R}^{3 \times 4}$ encodes the horizontal-plane geometry, and $\boldsymbol{\Gamma} = \mathrm{diag}(\gamma_1, \gamma_2, \gamma_3, \gamma_4) \in \mathbb{R}^{4 \times 4}$ models per-thruster effectiveness with $\gamma_i \in [0, 1]$. A misalignment of thruster i by angle θ_i is captured *column-wise* by

$$\boldsymbol{T}(\boldsymbol{\theta}) = [\boldsymbol{t}_1,\ \ldots,\ \boldsymbol{R}(\theta_i)\boldsymbol{t}_i,\ \ldots,\ \boldsymbol{t}_4],$$

with planar rotation $\boldsymbol{R}(\theta_i)$. Nominal operation corresponds to $\gamma_i = 1, \theta_i = 0$; a blocked thruster has $\gamma_i = 0$.

C. Control Objective and Standing Assumptions

The objective is to design a fault-tolerant tracking controller that achieves high-accuracy tracking in nominal conditions, and detects and accommodates thruster faults with minimal delay, and reallocates control effort while preserving closed-loop stability under thruster degradation. We make the following standard assumptions:

- $\boldsymbol{M} \succ 0$, $\exists\, d_{\min} > 0$ s.t. $\boldsymbol{D}(\boldsymbol{\nu}) \succeq d_{\min}\boldsymbol{I}\quad \forall\, \boldsymbol{\nu} = [u, v, r]^\top$ with $|u| \leq \bar{u}$, $|v| \leq \bar{v}$, $|r| \leq \bar{r}$. where $\bar{\boldsymbol{\nu}} = [\bar{u}, \bar{v}, \bar{r}]^\top$ denotes the operating-range bounds on the body-frame velocities.
- disturbances $\boldsymbol{w}$ are bounded; inputs $\boldsymbol{u} \in [\boldsymbol{u}_{\min}, \boldsymbol{u}_{\max}]$ with known rate limits;
- $(\boldsymbol{\Gamma}, \boldsymbol{\theta})$ are piecewise-constant and change at isolated instants (Sec. IV).

The constant $d_{\min} > 0$ is a uniform damping lower bound. Let $\boldsymbol{x}_d = [\boldsymbol{\eta}_d^\top, \boldsymbol{\nu}_d^\top]^\top$ denote the desired trajectory and its compatible body-frame velocity, with

$$\boldsymbol{\nu}_d = \boldsymbol{J}^{-1}(\psi_d)\,\dot{\boldsymbol{\eta}}_d, \tag{6}$$

Define the tracking error $\tilde{\boldsymbol{x}} = \boldsymbol{x} - \boldsymbol{x}_d$.

D. Augmented Error Model

To explicitly capture *persistent, low–frequency mismatches*—such as steady currents, unmodeled hydrodynamic loads, or residual allocation errors—we introduce a slowly varying bias in the generalized-force channel and treat it as an augmented state. This bias acts like a integral action inside MPC: it cancels constant/slow disturbances to remove steady-state offset, while remaining bounded when the mismatch disappears. We augment the generalized force with a bias $\boldsymbol{d} \in \mathbb{R}^{3 \times 1}$:

$$
\begin{aligned}
\boldsymbol{\tau}_{\text{eff}} &= \boldsymbol{T}(\boldsymbol{\theta})\boldsymbol{\Gamma}\,\boldsymbol{u} + \boldsymbol{d}, \\
\dot{\boldsymbol{d}} &= -\boldsymbol{\Lambda}\boldsymbol{d}, \quad \boldsymbol{\Lambda} = \mathrm{diag}(\lambda_i) \succ 0.
\end{aligned} \tag{7}
$$

Here $\boldsymbol{\Lambda}$ sets the bias dynamics: each $\lambda_i > 0$ is a designer-chosen decay rate (units s^{-1}), with time constant $\tau_i = 1/\lambda_i$. Small λ_i lets $\boldsymbol{d}$ track slow drifts; larger λ_i makes $\boldsymbol{d}$ decay faster. In practice, choose τ_i on the order of several sampling periods but slower than the dominant closed-loop bandwidth.

Using (4), (5), (6), and (7), the augmented error dynamics become

$$
\dot{\tilde{\boldsymbol{x}}} = \begin{bmatrix} \boldsymbol{J}(\psi)\boldsymbol{\nu} - \dot{\boldsymbol{\eta}}_d \\ \boldsymbol{M}^{-1}\big(\boldsymbol{\tau}_{\text{eff}} - \boldsymbol{C}(\boldsymbol{\nu})\boldsymbol{\nu} - \boldsymbol{D}(\boldsymbol{\nu})\boldsymbol{\nu}\big) - \dot{\boldsymbol{\nu}}_d \end{bmatrix} + \boldsymbol{w}, \tag{8}
$$

where the residual $\boldsymbol{w}$ collects fast, zero-mean disturbances not captured by $\boldsymbol{d}$. and the augmented state is $\tilde{\boldsymbol{x}}_{\text{aug}} = \begin{bmatrix} \tilde{\boldsymbol{x}}^{\top} & \boldsymbol{d}^{\top} \end{bmatrix}^{\top}$. The bias dynamics in (7) act as an integral action in the generalized-force domain: constant or slowly varying disturbances are absorbed by $\boldsymbol{d}$, enabling offset-free tracking while guaranteeing that $\boldsymbol{d}$ decays when no longer needed. This augmented model will be used in the LMPC design (Sec. III-B) and in the multi-model estimator (Sec. IV).

III. ADAPTIVE LYAPUNOV-BASED MPC DESIGN

Building on the formulation in Sec. II, we design a fault-tolerant controller as a *Lyapunov-Constrained MPC* posed on the 6-state tracking-error model. The augmentation captures slow-varying disturbances and model mismatch, preventing steady-state offsets under thruster degradation. A model-consistent online reconfiguration of the thrust effectiveness is embedded, so that constraints and allocation remain feasible under faults. Stability is enforced via a Lyapunov contraction constraint that each MPC must satisfy.

A. Architecture Overview

Fig 2 illustrates the overall control architecture, which integrates Bayesian mode estimation with LMPC to achieve fault-tolerant thrust allocation. A bank of Unscented Kalman Filters (UKFs) runs in parallel, each assuming a different thruster fault model. At each time step a Bayesian estimator fuses the UKF outputs to compute posterior probabilities of each mode. Each hypothesized mode is paired with its own LMPC controller, which is designed based on the corresponding fault model. Crucially, all mode-conditioned LMPC controllers share a common Lyapunov function pair and a shared contraction constraint, so that recursive feasibility and closed-loop stability are guaranteed regardless of which controller is active. Depending on the estimated mode probabilities, the system
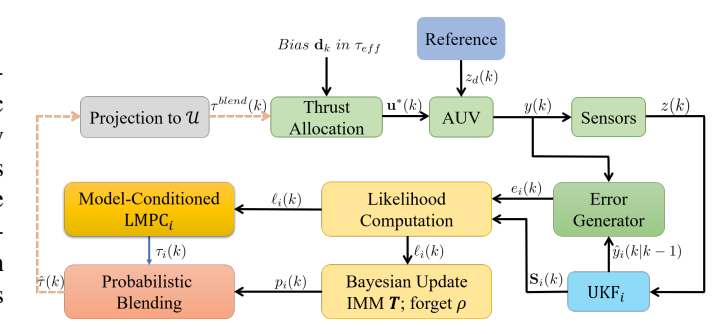

Fig. 2. Bayesian multi-model LMPC architecture. Each model uses the same first-step Lyapunov contraction and amplitude/rate limits, with generalized forces $\boldsymbol{\tau} = \boldsymbol{T}(\boldsymbol{\theta})\boldsymbol{\Gamma}\boldsymbol{u}$. An IMM Bayesian filter computes posterior probabilities for probability-weighted blending of the LMPC outputs.

either selects the controller for the most likely mode (MAP selection) or forms a "soft" blend of the controllers' outputs weighted by those probabilities.

This design is novel in combining Bayesian adaptation with LMPC for thrust control under faults. By embedding thrust allocation directly into the LMPC optimization and enforcing a Lyapunov-inspired contraction constraint, the scheme inherits the stability properties of the base Lyapunov controller. In effect, the MPC optimizer adjusts thrust commands online for best performance while respecting physical limits, and the contraction constraint ensures closed-loop stability. This integrated approach is simpler and more flexible than architectures that cascade separate fault-tolerant loops. In this approach, the controller passively adapts to each modeled failure mode without the need for explicit fault detection or reconfiguration. Building on the above architecture, we derive the mode-conditioned LMPC.

B. Lyapunov-Constrained MPC with First-Step Contraction

We now integrate a Lyapunov-based constraint into MPC so that the optimal control inherits the stabilizing behavior of a nonlinear auxiliary controller while optimizing performance. The derivation follows the backstepping construction in [14], [25], [26], [28], [32], extended here to the augmented bias state and online allocation.

Let the output position tracking error be $\tilde{\boldsymbol{\eta}} = \boldsymbol{\eta} - \boldsymbol{\eta}_d$. Define the virtual derivative reference and the *velocity error*

$$
\dot{\boldsymbol{\eta}}_r = \dot{\boldsymbol{\eta}}_d - \tilde{\boldsymbol{\eta}}, \qquad \boldsymbol{s} = \dot{\boldsymbol{\eta}} - \dot{\boldsymbol{\eta}}_r = \dot{\tilde{\boldsymbol{\eta}}} + \tilde{\boldsymbol{\eta}}. \tag{9}
$$

Using $\dot{\boldsymbol{\eta}} = \boldsymbol{R}(\psi)\boldsymbol{v}$, one has $\dot{\tilde{\boldsymbol{\eta}}} = \boldsymbol{s} - \tilde{\boldsymbol{\eta}}$. Let $\boldsymbol{v}_r = \boldsymbol{R}^{\top}(\psi)\dot{\boldsymbol{\eta}}_r$. Consider

$$
V_1 = \tfrac{1}{2}\,\tilde{\boldsymbol{\eta}}^{\top}\boldsymbol{K}_p\tilde{\boldsymbol{\eta}}, \quad V_2 = \tfrac{1}{2}\,\boldsymbol{s}^{\top}\boldsymbol{M}^*(\psi)\boldsymbol{s} + V_1, \tag{10}
$$

with $\boldsymbol{K}_p = \boldsymbol{K}_p^{\top} \succ 0$ and $\boldsymbol{M}^*(\psi) = \boldsymbol{R}(\psi)\boldsymbol{M}\,\boldsymbol{R}^{\top}(\psi)$. Taking time derivative of V_2 and Substituting the dynamics (3) results in [26], [28], [34]:

$$
\begin{aligned}
\dot{V}_2 = &-\mathbf{s}^{\top}[\mathbf{C}^*(\mathbf{v}, \psi) + \mathbf{D}^*(\mathbf{v}, \psi)]\mathbf{s} + \mathbf{s}^{\top}\mathbf{R}(\psi) \\
&\times [\boldsymbol{\tau} - \mathbf{M}\dot{\mathbf{v}}_r - \mathbf{C}(\mathbf{v})\mathbf{v}_r - \mathbf{D}(\mathbf{v})\mathbf{v}_r] \\
&+ \tfrac{1}{2}\mathbf{s}^{\top}\dot{\mathbf{M}}^*(\psi)\mathbf{s} - \tilde{\boldsymbol{\eta}}^{\top}\mathbf{K}_p\tilde{\boldsymbol{\eta}} + \mathbf{s}^{\top}\mathbf{K}_p\tilde{\boldsymbol{\eta}}
\end{aligned} \tag{11}
$$

where $\mathbf{C}^*(\mathbf{v}, \psi) = \mathbf{R}(\psi)[\mathbf{C}(\mathbf{v}) - \mathbf{M}\mathbf{R}^\top(\psi)\dot{\mathbf{R}}(\psi)]\mathbf{R}^\top(\psi)$ and $\mathbf{D}^*(\mathbf{v}, \psi) = \mathbf{R}(\psi)\mathbf{D}(\mathbf{v})\mathbf{R}^\top(\psi)$.

Because $\boldsymbol{C}(\boldsymbol{\nu}) = -\boldsymbol{C}^\top(\boldsymbol{\nu})$, we obtain

$$\mathbf{s}^\top(\dot{\mathbf{M}}^*(\psi) - 2\mathbf{C}^*(\mathbf{v}, \psi))\mathbf{s} = 0 \quad \forall \, \mathbf{v}, \, \psi \, , \mathbf{s} \qquad (12)$$

Using standard Euler–Lagrange identities, the auxiliary generalized-force law [27], [34], [35]

$$\boldsymbol{\tau}_b = \boldsymbol{M}\dot{\boldsymbol{v}}_r + \boldsymbol{C}(\boldsymbol{v})\boldsymbol{v}_r + \boldsymbol{D}(\boldsymbol{v})\boldsymbol{v}_r - \boldsymbol{R}^\top(\psi)\big(\boldsymbol{K}_p\tilde{\boldsymbol{\eta}} + \boldsymbol{K}_d\boldsymbol{s}\big), \quad (13)$$

with $\boldsymbol{K}_d = \boldsymbol{K}_d^\top \succ 0$, yields the decay

$$\dot{V}_2 = -\boldsymbol{s}^\top\big[\boldsymbol{D}^*(\boldsymbol{v}, \psi) + \boldsymbol{K}_d\big]\boldsymbol{s} - \tilde{\boldsymbol{\eta}}^\top\boldsymbol{K}_p\tilde{\boldsymbol{\eta}} \leq 0, \quad (14)$$

To capture slow-varying mismatch, we augment the generalized force with a bias $\boldsymbol{d}$ as in (7), and define the composite Lyapunov function

$$V(\tilde{\boldsymbol{\eta}}, \boldsymbol{s}, \boldsymbol{d}) = V_2(\tilde{\boldsymbol{\eta}}, \boldsymbol{s}) + \tfrac{1}{2}\,\boldsymbol{d}^\top\boldsymbol{P}_d\boldsymbol{d}, \quad \boldsymbol{P}_d = \boldsymbol{P}_d^\top \succ 0, \quad (15)$$

where $\dot{\boldsymbol{d}} = -\boldsymbol{\Lambda}\boldsymbol{d}$ with $\boldsymbol{\Lambda} \succ 0$ contributes $-\boldsymbol{d}^\top\boldsymbol{P}_d\boldsymbol{\Lambda}\boldsymbol{d}$ to $\dot{V}$.

Let $\boldsymbol{\xi} = [\tilde{\boldsymbol{\eta}}^\top, \boldsymbol{s}^\top, \boldsymbol{d}^\top]^\top$ and sampling period Δt. The MPC predictor uses the explicit Euler discretization [36]

$$\boldsymbol{\xi}_{k+1} = \boldsymbol{\xi}_k + \Delta t \, \tilde{\boldsymbol{f}}(\boldsymbol{\xi}_k, \boldsymbol{u}_k; \, \boldsymbol{T}(\boldsymbol{\theta}_k), \boldsymbol{\Gamma}_k), \qquad (16)$$

where $\tilde{\boldsymbol{f}}$ collects the error dynamics implied by (8) and the allocation (7).

Using V as terminal penalty, the Optimal Control Problem (OCP) at time k is

$$\min_{\{\boldsymbol{u}_{k+i}\}_{i=0}^{N-1}} \sum_{i=0}^{N-1} \Big(\|\tilde{\boldsymbol{\eta}}_{k+i}\|_{\boldsymbol{Q}_\eta}^2 + \|\boldsymbol{s}_{k+i}\|_{\boldsymbol{Q}_s}^2 + \|\boldsymbol{d}_{k+i}\|_{\boldsymbol{Q}_d}^2$$

$$+ \|\Delta\boldsymbol{u}_{k+i}\|_{\boldsymbol{R}}^2\Big) + V(\tilde{\boldsymbol{\eta}}_{k+N}, \boldsymbol{s}_{k+N}, \boldsymbol{d}_{k+N}) \quad (17)$$

$$\text{s.t.} \ \ \boldsymbol{\xi}_{k+i+1} = \boldsymbol{\xi}_{k+i} + \Delta t \, \tilde{\boldsymbol{f}}(\boldsymbol{\xi}_{k+i}, \boldsymbol{u}_{k+i}), \ \ i = 0{:}N{-}1,$$

$$\boldsymbol{\tau}_{k+i} = \boldsymbol{T}(\boldsymbol{\theta}_k)\boldsymbol{\Gamma}_k\,\boldsymbol{u}_{k+i},$$

$$\boldsymbol{u}_{\min} \leq \boldsymbol{u}_{k+i} \leq \boldsymbol{u}_{\max}, \ \ \|\Delta\boldsymbol{u}_{k+i}\|_\infty \leq \dot{\boldsymbol{u}}_{\max}\Delta t,$$

$$\underbrace{V(\boldsymbol{\xi}_{k+1}) - V(\boldsymbol{\xi}_k) \leq -\alpha\|\tilde{\boldsymbol{\eta}}_k\|^2}_{\text{Lyapunov descent at the first step}}, \ \alpha > 0,$$

$$\boldsymbol{\xi}_{k+N} \in \mathcal{X}_f = \{\boldsymbol{\xi} : V(\boldsymbol{\xi}) \leq c\}.$$

Terminal set. In this work we choose a small $c > 0$ so that $\mathcal{X}_f = \{\boldsymbol{\xi} : V(\boldsymbol{\xi}) \leq c\}$ lies within the local region of attraction(ROA) of the auxiliary backstepping feedback and respects input/rate constraints; this set is obtained numerically. The *first-step* descent inequality enforces that the MPC's initial move decreases V at least by $\alpha\|\tilde{\boldsymbol{\eta}}_k\|^2$, matching the decay of the auxiliary law (13). The terminal set $\mathcal{X}_f$ is chosen positively invariant under (13) with the *faulty* mapping $\boldsymbol{T}(\boldsymbol{\theta})\boldsymbol{\Gamma}$.

C. Online Reconfiguration of Thrust Effectiveness

We model thruster faults by *column-wise scaling and in-plane rotation* of the thrust mapping (see Sec. II for the parameterization). Let $\boldsymbol{T} = [\boldsymbol{t}_1 \ \boldsymbol{t}_2 \ \boldsymbol{t}_3 \ \boldsymbol{t}_4] \in \mathbb{R}^{3\times4}$ be the nominal allocation and $\boldsymbol{\Gamma} = \mathrm{diag}(\gamma_1, \ldots, \gamma_4)$ with $\gamma_i \in [0, 1]$. If thruster i is misaligned by θ_i and derated, we form the rotated mapping

$$\tilde{\boldsymbol{T}}(\boldsymbol{\theta}) = [\boldsymbol{t}_1, \ldots, \boldsymbol{R}(\theta_i)\boldsymbol{t}_i, \ldots, \boldsymbol{t}_4], \ \boldsymbol{\tau}_k = \tilde{\boldsymbol{T}}(\boldsymbol{\theta}_k)\,\boldsymbol{\Gamma}_k\,\boldsymbol{u}_k, \ (18)$$

where $\boldsymbol{R}(\theta_i)$ denotes the planar rotation applied to the ith column.

At each sampling instant k, the OCP in (17) is updated with the current $\tilde{\boldsymbol{T}}(\boldsymbol{\theta}_k)$ and $\boldsymbol{\Gamma}_k$. Per-thruster bounds are tightened to reflect the remaining capability; in particular, if $\gamma_i = 0$ then $u_{i,k} = 0$. Feasibility is enforced by the amplitude and rate limits in (17).

We warm-start the solver with a least-squares allocation

$$\boldsymbol{u}_k^{\mathrm{init}} = \big(\tilde{\boldsymbol{T}}(\boldsymbol{\theta}_k)\,\boldsymbol{\Gamma}_k\big)^\dagger \boldsymbol{\tau}_k, \qquad (19)$$

or, for numerical robustness, with a damped least-squares form

$$\boldsymbol{u}_k^{\mathrm{init}} = \big(\tilde{\boldsymbol{T}}(\boldsymbol{\theta}_k)\,\boldsymbol{\Gamma}_k\big)^\top \Big(\tilde{\boldsymbol{T}}(\boldsymbol{\theta}_k)\,\boldsymbol{\Gamma}_k\big(\tilde{\boldsymbol{T}}(\boldsymbol{\theta}_k)\,\boldsymbol{\Gamma}_k\big)^\top + \varepsilon\boldsymbol{I}\Big)^{-1}\boldsymbol{\tau}_k,$$

Where $\varepsilon > 0$. Because the first-step Lyapunov contraction in (17) is evaluated using the *current* mapping $\tilde{\boldsymbol{T}}(\boldsymbol{\theta}_k), \boldsymbol{\Gamma}_k$, reconfiguration does not alter the contraction condition. It only changes the admissible input set and the predicted generalized force, while the enforced decrease of V at the first step remains in force.

IV. BAYESIAN MULTI-MODEL ADAPTIVE FAULT-TOLERANT FRAMEWORK

After establishing the single-model LMPC with a common Lyapunov contraction constraint, we now describe the Bayesian multi-model adaptation layer that provides online fault diagnosis and controller blending. The key idea is to run a bank of mode-conditioned estimators and LMPCs, update the posterior probabilities of the modes from measurement innovations, and fuse the candidate control actions using these posteriors to achieve *soft switching* with stability guarantees.

A. Multi-Model Parameterization

We adopt a discrete set of mode hypotheses

$$\mathcal{M} = \{I, II, III\}, \qquad (20)$$

where each mode $i \in \mathcal{M}$ is characterized by the thruster effectiveness and possible misalignment parameters

$$\Theta_i = \{\Gamma_i, \theta_i\}, \ \Gamma_i = \mathrm{diag}(\gamma_{1,i}, \ldots, \gamma_{4,i}) \in [0, 1]^{4\times4}, \quad (21)$$

and the column-wise rotated allocation matrix are described in (18). The plant dynamics in mode i keep the *same* nonlinear structure as in Sec. II, changing only through the generalized force mapping

$$\boldsymbol{\tau} = \tilde{\boldsymbol{T}}(\theta_i)\boldsymbol{\Gamma}_i\,\boldsymbol{u}, \qquad \boldsymbol{\tau}_{\mathrm{eff}} = \boldsymbol{\tau} + \boldsymbol{d}, \qquad (22)$$

with the same augmented bias dynamics $\dot{\boldsymbol{d}} = -\boldsymbol{\Lambda}\boldsymbol{d}$. Throughout this section, the LMPC layer per mode i uses the identical cost and constraints as Sec. III-B.

B. Bayesian Posterior Probability Update

Each mode i runs a UKF that provides the one-step predicted output $\hat{y}_i(k|k-1)$ and innovation covariance $S_i(k)$. We update the posterior probabilities $p_i(k)$ via an IMM prior and a Gaussian log-likelihood, and we use probability-weighted blending of mode-conditioned LMPC outputs [37] . Let the innovation be

$$e_i(k) = y(k) - \hat{y}_i(k|k-1). \qquad (23)$$

Assuming Gaussian measurement noise, the instantaneous log-likelihood [31], [38] is computed as

$$\ell_i(k) = -\tfrac{1}{2}\left[e_i^\top S_i^{-1} e_i + \log \det S_i + p \log(2\pi)\right], \qquad (24)$$

where $p = \dim(y(k))$. To prevent numerical singularity when S_i is ill-conditioned, a small $\varepsilon > 0$ is added to the diagonal, i.e., $S_i \leftarrow S_i + \varepsilon I$.

To suppress chattering in probability evolution caused by transient noise, we apply an exponentially weighted cumulative log-likelihood [39]:

$$\bar{\ell}_i(k) = \rho\, \bar{\ell}_i(k-1) + \ell_i(k), \quad \rho \in (0,1], \qquad (25)$$

where ρ is a forgetting factor. When $\rho = 1$, all past likelihoods are equally weighted; smaller ρ values discount older measurements.

Slow mode transitions are modeled by a first-order Markov chain with transition matrix $T_{ji} = \Pr\{m(k) = i \mid m(k-1) = j\}$, which yields the mixed prior probability [31], [40], [41]:

$$\tilde{p}_i(k) = \sum_{j \in \mathcal{M}} T_{ji}\, p_j(k-1). \qquad (26)$$

This is equivalent to the mode interaction step in the Interacting Multiple Model (IMM) filter [42].

Applying Bayes' theorem, the posterior probability is

$$p_i(k) = \frac{\tilde{p}_i(k)\, \exp\{\bar{\ell}_i(k)\}}{\sum_{r \in \mathcal{M}} \tilde{p}_r(k)\, \exp\{\bar{\ell}_r(k)\}}, \quad \sum_i p_i(k) = 1. \qquad (27)$$

For improved numerical stability, especially when $\bar{\ell}_i(k)$ is large in magnitude, (27) is computed in the log domain using the log-sum-exp technique [43]:

$$\hat{\ell}_i(k) = \log \tilde{p}_i(k) + \bar{\ell}_i(k), \quad m = \max_{r \in \mathcal{M}} \hat{\ell}_r(k), \qquad (28)$$

$$p_i(k) = \frac{\exp\{\hat{\ell}_i(k) - m\}}{\sum_{r \in \mathcal{M}} \exp\{\hat{\ell}_r(k) - m\}}. \qquad (29)$$

This approach preserves probability normalization and avoids underflow or overflow in floating-point computation.

C. Control Fusion and Supervisory Logic

At each sampling instant, the mode–conditioned LMPC for $i \in \mathcal{M}$ returns a feasible input $\boldsymbol{u}_i^\star(k)$ and the corresponding generalized force $\boldsymbol{\tau}_i^\star(k) = \boldsymbol{T}(\theta_i)\boldsymbol{\Gamma}_i \boldsymbol{u}_i^\star(k)$. We apply a *probabilistic blending* of these candidates which form the convex combination in force space [33], [44], [45]

$$\boldsymbol{\tau}^{\text{blend}}(k) = \sum_{i \in \mathcal{M}} p_i(k)\, \boldsymbol{\tau}_i^\star(k), \qquad (30)$$

and map it to thruster commands via a least–squares allocation using the current most–probable parameters $(\bar{\theta}, \bar{\Gamma}) = \arg\max_i p_i(k)$:

$$\hat{\boldsymbol{u}}(k) = \left(\boldsymbol{T}(\bar{\theta})\bar{\boldsymbol{\Gamma}}\right)^\dagger \boldsymbol{\tau}^{\text{blend}}(k), \quad \boldsymbol{u}^{\text{blend}}(k) = \Pi_{\mathcal{U}}\big(\hat{\boldsymbol{u}}(k)\big), \quad (31)$$

where $\Pi_{\mathcal{U}}$ denotes projection onto the admissible input set. This procedure yields smooth control during probability transitions and guarantees feasibility by construction through $\Pi_{\mathcal{U}}$.

For each mode i, the associated LMPC enforces the same first–step contraction

$$V(F(\boldsymbol{\xi}_k, \boldsymbol{u}_i^\star)) - V(\boldsymbol{\xi}_k) \leq -\alpha\|\tilde{\boldsymbol{x}}_k\|^2, \quad \alpha > 0. \qquad (32)$$

Over one prediction step, the augmented error dynamics are affine in the generalized force and $V(\cdot)$ is quadratic; hence for the unprojected blend $\hat{\boldsymbol{u}}$ one has the Jensen-type bound

$$V(F(\boldsymbol{\xi}_k, \hat{\boldsymbol{u}})) \leq \sum_{i \in \mathcal{M}} p_i(k)\, V(F(\boldsymbol{\xi}_k, \boldsymbol{u}_i^\star)). \qquad (33)$$

Combining (32)–(33) and $\sum_i p_i = 1$ yields

$$V(F(\boldsymbol{\xi}_k, \hat{\boldsymbol{u}})) - V(\boldsymbol{\xi}_k) \leq -\alpha\|\tilde{\boldsymbol{x}}_k\|^2. \qquad (34)$$

If $\hat{\boldsymbol{u}}$ is feasible, the applied $\boldsymbol{u}^{\text{blend}} = \hat{\boldsymbol{u}}$ preserves the exact contraction (34). If projection is active, Lipschitz continuity of $V \circ F$ in $\boldsymbol{u}$ implies

$$V\big(F(\boldsymbol{\xi}_k, \boldsymbol{u}^{\text{blend}})\big) - V(\boldsymbol{\xi}_k) \leq -\alpha\|\tilde{\boldsymbol{x}}_k\|^2 + L_u\, \|\boldsymbol{u}^{\text{blend}} - \hat{\boldsymbol{u}}\|, \qquad (35)$$

for some $L_u > 0$ depending on local model bounds. Since $\Pi_{\mathcal{U}}$ is a nonexpansive projection and rate limits bound $\|\boldsymbol{u}^{\text{blend}} - \hat{\boldsymbol{u}}\|$, the contraction margin remains negative provided $L_u \|\boldsymbol{u}^{\text{blend}} - \hat{\boldsymbol{u}}\| \leq \alpha'\|\tilde{\boldsymbol{x}}_k\|^2$ for a chosen $\alpha' \in (0, \alpha)$. In practice, this is ensured by the shared auxiliary backstepping rate embedded in (32), and conservative rate limits, so recursive feasibility and closed-loop stability are maintained during probability evolution. To reduce computation without affecting stability, one may temporarily switch to the most–probable controller when $p_m(k) \geq p_{\text{on}}$ for N_{on} samples, and resume blending only if $p_m(k) \leq p_{\text{off}} < p_{\text{on}}$ for N_{off} samples. Anomaly-triggered "unlocking" can be used to avoid probability lock-in under new faults.

V. SIMULATIONS AND RESULTS

To demonstrate the effectiveness and fault-tolerant capability of the proposed ALMPC framework, we conduct numerical simulations on the AUV model. All simulations are implemented in MATLAB R2023b. Model and controller parameters follow the Saab Seaeye Falcon specifications [26], [32], [34].

A. Simulation Settings

Three representative AUV modes are considered:
- **Model I (nominal)** $\gamma_i = 1, \theta_i = 0$;
- **Model II (thruster #1 failure)** $\gamma_1 = 0$;
- **III (thruster #3 misaligned + derated)** $\gamma_3 = 0.3$, column t_3 rotated by $\theta_3 = 15°$.

This parameterization directly matches the thrust mapping in Sec. II and the LMPC constraints in Sec. III-B. Two scenarios

are evaluated: **Case I**: Model I → Model II at $t = 15$ s. The reference trajectory is

$$p(t) = \begin{cases} x_d = 0.5\ t, \\ y_d = \sin(0.5\ t). \end{cases}$$

Case II: Model I → Model II at $t = 10$ s, then Model II → Model III at $t = 20$ s. The reference is an eight-shaped path

$$p(t) = \begin{cases} x_d = -\sin(0.5\ t), \\ y_d = \sin(0.25\ t). \end{cases}$$

Unless otherwise stated, the controller uses sampling time $\Delta t = 0.1$ s and prediction horizon $N = 10$. The LMPC weights follow [32]

$$Q = \text{diag}(10^5, 10^5, 10^3, 10^2, 10^2, 10^2)$$
$$R = \text{diag}(10^{-4}, 10^{-4}, 10^{-4}, 10^{-4})$$
$$Q_f = \text{diag}(10^3, 10^3, 10^2, 10, 10, 10).$$

The UKF covariances are

$$Q_{\text{ukf}} = \text{blkdiag}(0.01, 0.01, 0.01,\ 0.005, 0.005, 0.005)$$
$$R_{\text{ukf}} = \text{diag}(0.1, 0.1, 0.1,\ 0.03, 0.03, 0.03).$$

Thruster amplitude limits are ± 500 N. The initial state is $x(0) = [0.5, 0, 0, 0, 0, 0]^\top$. The baseline BSC gains are $K_p = K_d = \text{diag}(1, 1, 1)$. The LMPC problem in (17) is solved by discretizing the dynamics and applying SQP to the resulting Karush–Kuhn–Tucker (KKT) system [46]. Additionally, the Bayesian layer uses a first-order Markov prior with diagonal persistence $T_{\text{diag}} = 0.98$, i.e., $\boldsymbol{T} = T_{\text{diag}} \boldsymbol{I}_3 + \frac{1-T_{\text{diag}}}{2}(\mathbf{11}^\top - \boldsymbol{I}_3)$; the log-likelihood is exponentially weighted with $\rho = 0.9995$. To stress-test offset rejection we set the bias leakage in (7) to $\boldsymbol{\Lambda} = \boldsymbol{0}$. Supervisory switching uses hysteresis thresholds $p_{\text{on}} = 0.95$, $p_{\text{off}} = 0.80$ and dwell counts $N_{\text{on}} = 10$, $N_{\text{off}} = 5$. Detection time T_{det} is measured from the fault instant to the earliest time when the true-mode posterior exceeds $p_{\text{on}} = 0.95$ for $N_{\text{on}} = 10$ consecutive samples; accommodation time T_{acc} is measured to the earliest time when $|e_x|, |e_y| < 0.1$ m for at least 1 s.

B. Tracking Performance

Results for **Case I** are shown in Figures 3 and 4. The black solid curve is the reference, the blue dash-dot curve is BSC, and the red dashed curve is ALMPC. The vertical magenta line marks the switch at $t = 15$ s.

Before the fault, both BSC and ALMPC track well. After thruster #1 fails, BSC degrades markedly due to loss of control authority, whereas ALMPC swiftly reallocates thrust among healthy thrusters and preserves tight tracking; see the absolute errors in Fig 5. The x-axis error of BSC peaks near 1.0 m around $t = 24$ s, while ALMPC remains below 0.1 m; the y-axis error shows a similar gap (BSC up to 0.8 m vs. ALMPC < 0.05 m).

Thruster commands in Fig 6 highlight the effect of reallocation: BSC continues to request force from the failed thruster #1, wasting effort and distorting the trajectory, whereas ALMPC shifts demand to the remaining thrusters while respecting limits.
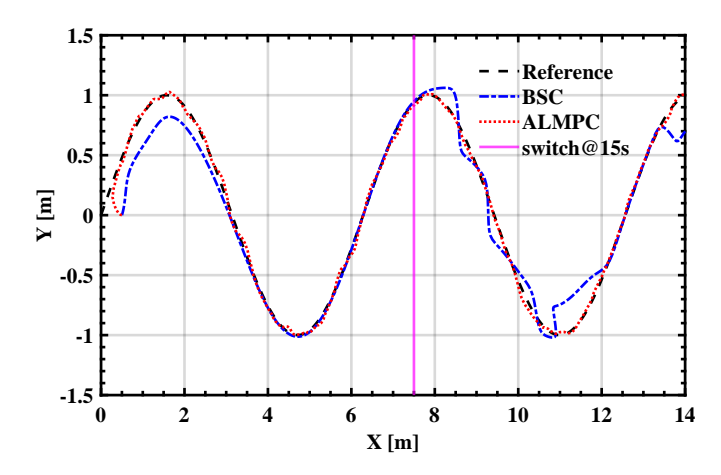

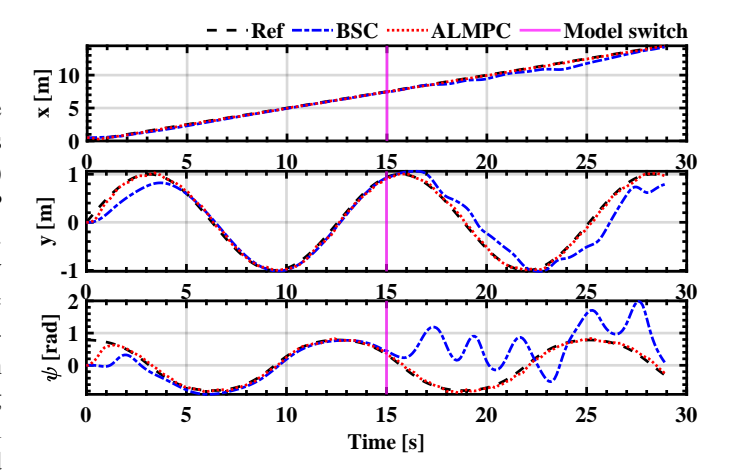Fig. 3. AUV trajectory in the XY plane under single-model switching.

Fig. 4. State trajectories (x, y, ψ) for single-model switching.
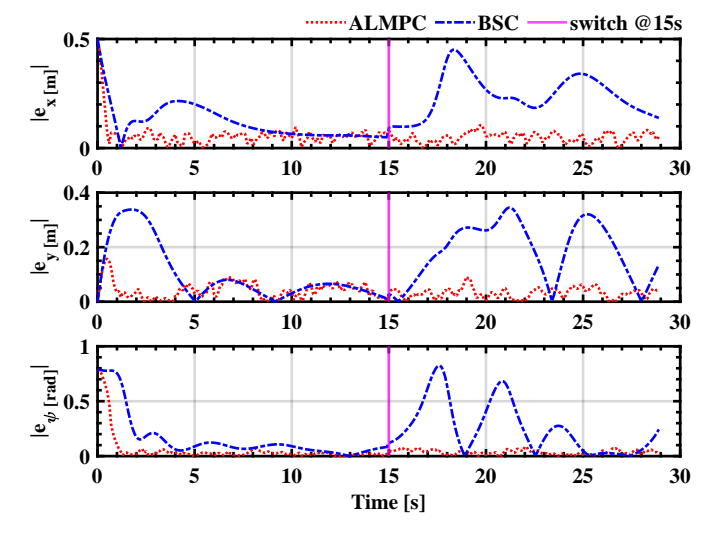

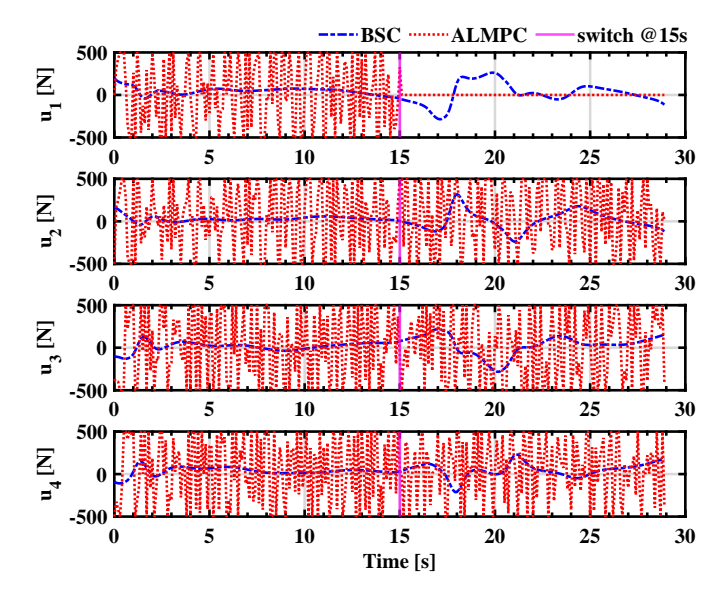Fig. 5. Absolute tracking errors under single-model switching.

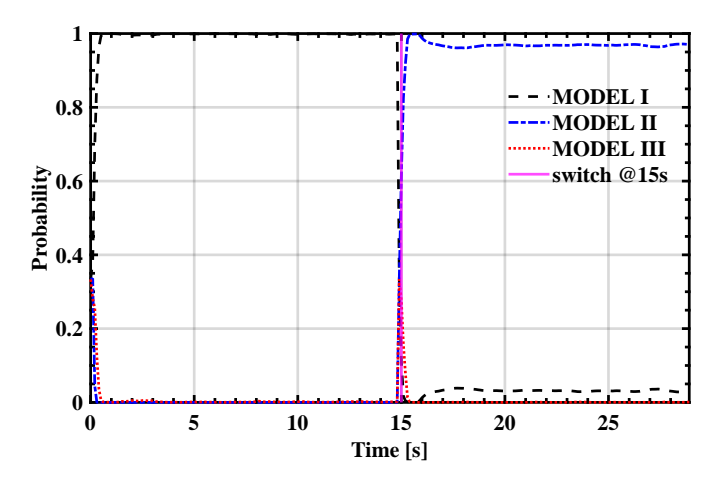Fig. 6. Thruster outputs under single-model switching.

Fig. 7. Model posterior probabilities for single-model switching.

The Bayesian identification is shown in Fig 7. The posterior, initially dominated by Model I, rapidly shifts after $t = 15$ s and exceeds 0.9 for Model II in about 1 s, while the other probabilities decay toward zero. During this transient, probability-weighted blending keeps the control smooth and prevents switching kicks. Using the supervisor's confirmation rule ($p_{\text{on}} = 0.95$, $N_{\text{on}} = 10$), the detection delay is $T_{\text{det}} \approx 0.3$ s. With the error band $(\varepsilon_\eta, \varepsilon_\psi) = (0.10 \text{ m}, 0.05 \text{ rad})$, the accommodation time is $T_{\text{acc}} \approx 0.3$ s.

C. Comparative Evaluation

We further compare ALMPC, (AMPC), and BSC under **Case II** . All estimation settings are identical to Case I. The posteriors in Fig 8 confirm rapid recognition: after the failure at $t = 10$ s, the probability of Model II exceeds 0.95 within 0.3 s (first switch) and 0.5 s (second switch) under the confirmation rule; following the second fault at $t = 20$ s, Model III becomes dominant with a similar time-to-confidence. For the first transition (I→II at t=10 s), the confirmation time is $T_{\text{det}} \approx 0.3$ s and the accommodation time
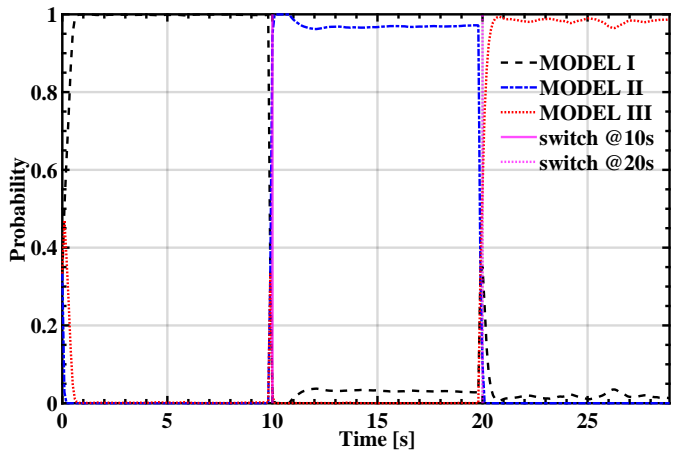

Fig. 8. Model posterior probabilities under multiple-model switching.
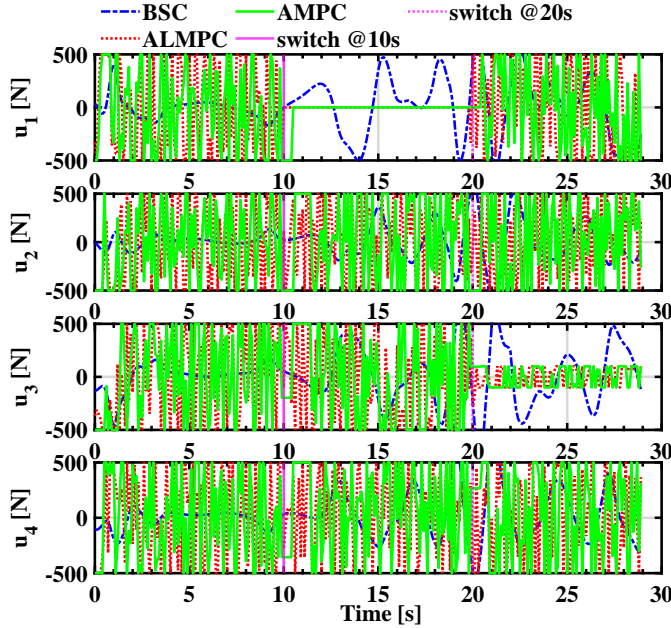

Fig. 9. Thruster outputs under multiple-model switching.

$T_{\text{acc}} \approx 0.3$ s. For the second transition (II→III at t=20 s), we obtain $T_{\text{det}} \approx 0.5$ s and $T_{\text{acc}} \approx 0.4$ s under the same criteria.

The thruster responses in Fig 9 make the reallocation explicit: BSC continues to command the failed thruster, while ALMPC increases the contribution of healthy thrusters (e.g., thruster #2) immediately after the failures.

Trajectory and state comparisons are given in Figures 10 and 11. Prior to 10 s, ALMPC and AMPC perform similarly, while BSC lags. At the fault instants (10 s and 20 s), *AMPC exhibits pronounced transients*, whereas *ALMPC remains smooth*. The absolute errors in Fig 12 show that ALMPC keeps deviations within 0.1 m in both x and y even during fault transitions, whereas AMPC peaks near 0.5 m and BSC exceeds 1 m.

At a fault instant, AMPC's internal model $\hat{\Theta}$ lags the true post-fault parameters $\Theta^\star$; hence the first control move is computed against a mismatched prediction/constraint set. Because
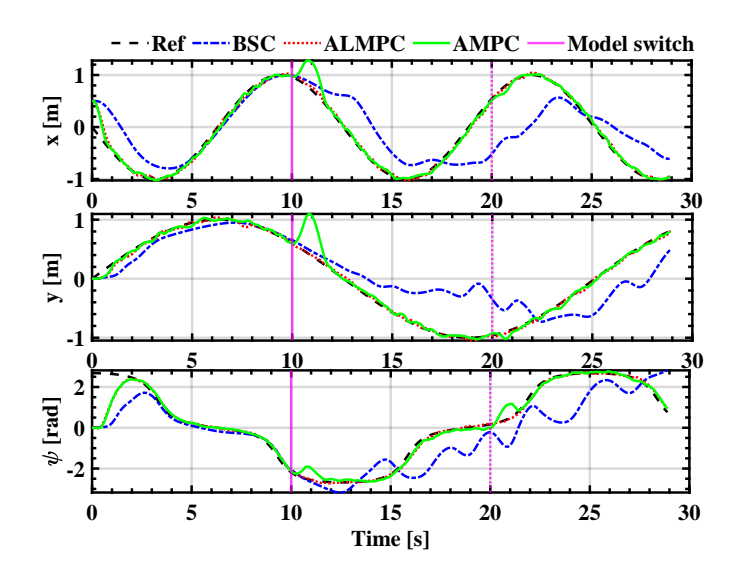
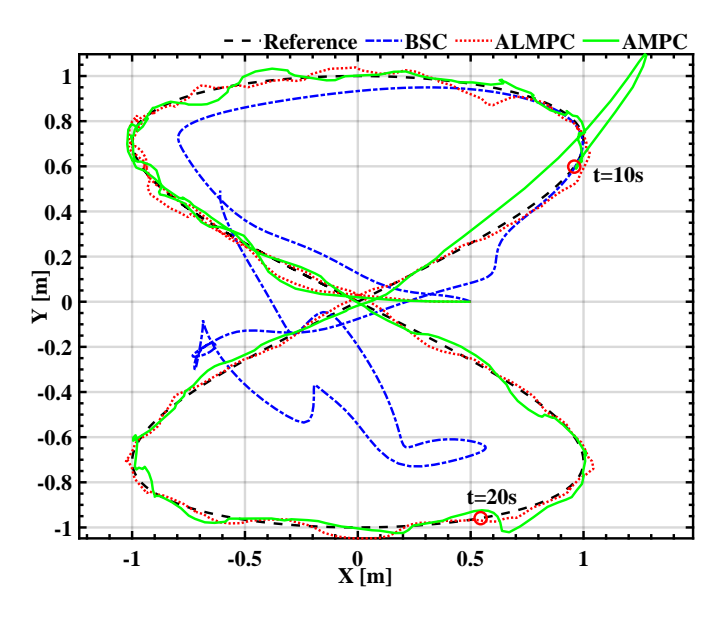Fig. 10. State trajectories (x, y, ψ) under multiple-model switching.

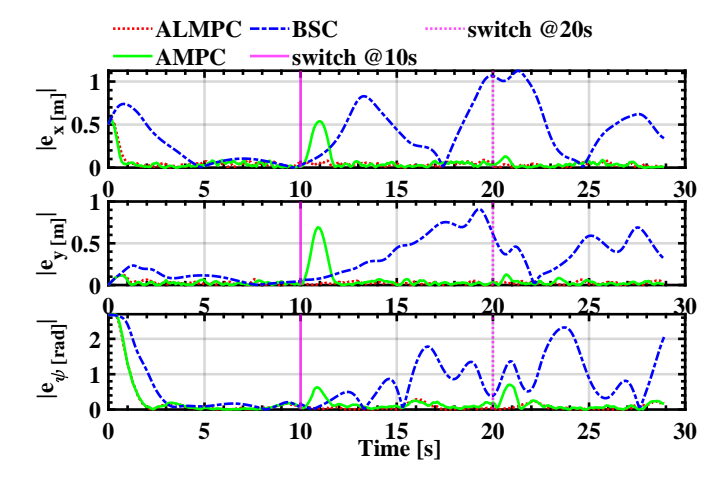Fig. 11. AUV trajectory in the XY plane under multiple-model switching.

Fig. 12. Absolute tracking errors for different control methods.

State	Metric	ALMPC	AMPC	BSC
x	RMSE	0.0799	0.1415	0.2704
	MaxAE	0.5501	0.6283	0.7402
	SSE	1.8531	5.8072	21.197
	IAE	1.2399	2.1132	5.8113
y	RMSE	0.0296	0.1072	0.1355
	MaxAE	0.1267	0.4857	0.3011
	SSE	0.2543	3.3333	5.3224
	IAE	0.6226	1.6552	3.2003
ψ	RMSE	0.4802	0.5646	0.6803
	MaxAE	2.6960	2.7014	2.6779
	SSE	66.857	92.444	134.200
	IAE	4.8767	7.8114	11.171

AMPC does not enforce a first-step Lyapunov contraction, $V(\xi_{k+1}) - V(\xi_k)$ may temporarily increase, manifesting as an overshoot and a sharp change in thrust. In contrast, each mode-conditioned LMPC in the proposed framework satisfies the *same* contraction inequality, and the applied input is the probability-weighted blend $\boldsymbol{u} = \sum_i p_i \boldsymbol{u}_i^*$, projected onto the admissible set. Since $\sum_i p_i = 1$, the convex combination preserves contraction, thus preventing switching kicks and keeping thrust continuous up to the enforced rate limits. Relative to AMPC, ALMPC reduces RMSE by 44% (x), 72% (y), and 15% (ψ), and cuts IAE by 41–62% across all states.

As summarized in Table I, ALMPC attains the lowest RMSE and MaxAE across all components while keeping the squared error (SSE) small, in agreement with the smooth, probability-weighted blending across Lyapunov-Constrained LMPCs. By contrast, AMPC's transients at the fault instants are consistent with the parameter lag and the absence of a first-step contraction bound.

VI. CONCLUSION

This work presented an ALMPC with a Bayesian multi-model layer for fault-tolerant AUV tracking. The design meets the three stated objectives: (i) high-accuracy nominal tracking via an augmented error–bias model that removes steady-state offsets; (ii) fast fault detection and accommodation through a UKF-driven Bayesian update and probabilistic blending—quantitatively, in Case II we obtained $T_{\text{det}}=\{0.3,\ 0.5\}$ s and $T_{\text{acc}}=\{0.3,\ 0.4\}$ s at the two switches; and (iii) stable thrust reallocation under degradation guaranteed by a shared first-step Lyapunov contraction across modes. Compared with AMPC and BSC, ALMPC delivered the lowest RMSE/MaxAE and significantly smaller SSE/IAE (Table I) while keeping commands smooth at mode transitions.

Future work will extend the mode set to continuous fault manifolds, develop tighter robustness margins for rapidly varying posteriors, and validate the approach in 6-DOF experiments and sea trials.

REFERENCES

[1] W. Bai, S. Zhang, X. Zhang, X. Ma, S. Yang, Y. Li, and T. Huang, "Exploring the generalizability of geomagnetic naviga-

tion: A deep reinforcement learning approach with policy distillation," *IEEE Transactions on Instrumentation and Measurement*, vol. 74, DOI 10.1109/TIM.2025.3598399, pp. 1–16, 2025.

[2] S. Yang, X. Zhang, S. Zhang, X. Ma, W. Bai, Y. Li, and T. Huang, "A bionic data-driven approach for long-distance underwater navigation with anomaly resistance," *IEEE Transactions on Instrumentation and Measurement*, vol. 74, DOI 10.1109/TIM.2025.3545179, pp. 1–14, 2025.

[3] W. Bai, X. Zhang, S. Zhang, S. Yang, Y. Li, and T. Huang, "Long-distance geomagnetic navigation in gnss-denied environments with deep reinforcement learning," *arXiv preprint arXiv:2410.15837*, 2024.

[4] S. Yang, S. Zhang, Q. Zhang, X. Zhang, and X. Ma, "Hardware-in-the-loop simulation testbed for geomagnetic navigation," *arXiv preprint arXiv:2412.11882*, 2024.

[5] T. I. Fossen, *Handbook of Marine Craft Hydrodynamics and Motion Control.* Wiley, Apr. 2021.

[6] D. Ma, Y. Li, T. Ma, and A. M. Pascoal, "The state of the art in key technologies for autonomous underwater vehicles: A review," *Engineering*, DOI 10.1016/j.eng.2025.08.002, Aug. 2025. [Online]. Available: https://www.sciencedirect.com/science/article/pii/S209580992500445X

[7] Z. Chu, Z. Gu, Y. Chen, D. Zhu, and J. Tang, "A fault diagnostic approach for underwater thrusters based on generative adversarial network," *IEEE Transactions on Instrumentation and Measurement*, vol. 73, DOI 10.1109/tim.2024.3417591, pp. 1–14, 2024.

[8] X. Chen, N. Bose, M. Brito, F. Khan, B. Thanyamanta, and T. Zou, "A review of risk analysis research for the operations of autonomous underwater vehicles," *Reliability Engineering & System Safety*, vol. 216, DOI 10.1016/j.ress.2021.108011, p. 108011, Dec. 2021.

[9] F. Liu, Z. Ma, B. Mu, C. Duan, R. Chen, Y. Qin, H. Pu, and J. Luo, "Review on fault-tolerant control of unmanned underwater vehicles," *Ocean Engineering*, vol. 285, DOI 10.1016/j.oceaneng.2023.115471, p. 115471, Oct. 2023.

[10] H. Liu, S. Zhang, S. Jiao, X. Zhang, X. Ma, Y. Yan, W. Cui, and Y. Zhang, "Adaptive fault-tolerant control of underwater vehicles with thruster failures," *arXiv preprint arXiv:2504.16037*, 2025.

[11] J. Liu, X. Wei, P. Qin, B. He, and C. Guedes Soares, "Cfd simulation and experimental validation of novel cutting device for underwater propeller entanglements," *Ocean Engineering*, vol. 309, DOI 10.1016/j.oceaneng.2024.118400, p. 118400, Oct. 2024. [Online]. Available: https://www.sciencedirect.com/science/article/pii/S0029801824017384

[12] Y. Li, J. He, H. Shen, W. Zhang, and Y. Li, "Adaptive practical prescribed-time fault-tolerant control for autonomous underwater vehicles trajectory tracking," *Ocean Engineering*, vol. 277, DOI 10.1016/j.oceaneng.2023.114263, p. 114263, Jun. 2023.

[13] X. Ma, S. Zhang, Y. Li, F. Qian, Z. Sun, and T. Huang, "Adaptive robust tracking control with active learning for linear systems with ellipsoidal bounded uncertainties," *IEEE Transactions on Automatic Control*, vol. 69, DOI 10.1109/TAC.2024.3410912, no. 11, pp. 8096–8103, 2024.

[14] Y. Wang and H. Zhang, "Lyapunov-based model predictive control for trajectory tracking of hovercraft with actuator constraints and external disturbances," *Ocean Engineering*, vol. 310, DOI 10.1016/j.oceaneng.2024.118631, p. 118631, Oct. 2024.

[15] X. Ma, Y. Chen, S. Zhang, Y. Li, F. Qian, and Z. Sun, "Robust quadratic optimal control of linear systems with ellipsoid-set learning," in *2024 European Control Conference (ECC)*, DOI 10.23919/ECC64448.2024.10591250, pp. 2125–2131, 2024.

[16] K. S. Narendra, O. A. Driollet, and K. George, *Adaptive Control Using Multiple Models: A Methodology*, pp. 83–110. Springer US, 2003.

[17] J. Hespanha and A. Morse, "Stability of switched systems with average dwell-time," in *Proceedings of the 38th IEEE Conference on Decision and Control (Cat. No.99CH36304)*, ser. CDC-99, vol. 3, DOI 10.1109/cdc.1999.831330, pp. 2655–2660. IEEE, 1999.

[18] X. Liu, B. Sun, and Z. Su, "Multi-mode fault-tolerant trajectory tracking control of auv under thruster failure conditions in complex environments," *Ocean Engineering*, vol. 330, DOI https://doi.org/10.1016/j.oceaneng.2025.121257, p. 121257, 2025. [Online]. Available: https://www.sciencedirect.com/science/article/pii/S0029801825009709

[19] H. Chen, G. Tang, S. Wang, W. Guo, and H. Huang, "Adaptive fixed-time backstepping control for three-dimensional trajectory tracking of underactuated autonomous underwater vehicles," *Ocean Engineering*, vol. 275, DOI https://doi.org/10.1016/j.oceaneng.2023.114109, p. 114109, 2023. [Online]. Available: https://www.sciencedirect.com/science/article/pii/S0029801823004936

[20] B. Li, X. Gao, H. Huang, and H. Yang, "Improved adaptive twisting sliding mode control for trajectory tracking of an auv subject to uncertainties," *Ocean Engineering*, vol. 297, DOI https://doi.org/10.1016/j.oceaneng.2023.116204, p. 116204, 2024. [Online]. Available: https://www.sciencedirect.com/science/article/pii/S002980182302588X

[21] X. Ma, S. Zhang, F. Qian, J. Wang, and L. Yan, "Q-learning based linear quadratic regulator with balanced exploration and exploitation for unknown systems," in *2022 China Automation Congress (CAC)*, DOI 10.1109/CAC57257.2022.10055961, pp. 446–451, 2022.

[22] S. Zhang, H. Cao, Y. Zhang, L. Jia, Z. Ye, and X. Hei, "Data-driven optimization framework for nonlinear model predictive control," *Mathematical Problems in Engineering*, vol. 2017, no. 1, p. 9402684, 2017.

[23] J. Wang, S. Zhang, J. Liu, X. Ma, and H. Liu, "Fine-tuning for data-enabled predictive control of noisy systems by reinforcement learning," *arXiv preprint arXiv:2505.24572*, 2025.

[24] H. Wei and Y. Shi, "Mpc-based motion planning and control enables smarter and safer autonomous marine vehicles: perspectives and a tutorial survey," *IEEE/CAA Journal of Automatica Sinica*, vol. 10, DOI 10.1109/jas.2022.106016, no. 1, pp. 8–24, Jan. 2023.

[25] C. Shen, Y. Shi, and B. Buckham, "Lyapunov-based model predictive control for dynamic positioning of autonomous underwater vehicles," in *2017 IEEE International Conference on Unmanned Systems (ICUS)*, DOI 10.1109/icus.2017.8278413, pp. 588–593. IEEE, Oct. 2017.

[26] C. Shen, "Motion control of autonomous underwater vehicles using advanced model predictive control strategy," Ph.D. dissertation, University of Victoria, 2018. [Online]. Available: http://hdl.handle.net/1828/9144

[27] C. Shen and Y. Shi, "Distributed implementation of nonlinear model predictive control for auv trajectory tracking," *Automatica*, vol. 115, DOI 10.1016/j.automatica.2020.108863, p. 108863, May. 2020.

[28] P. Gong, Z. Yan, W. Zhang, and J. Tang, "Lyapunov-based model predictive control trajectory tracking for an autonomous underwater vehicle with external disturbances," *Ocean Engineering*, vol. 232, DOI 10.1016/j.oceaneng.2021.109010, p. 109010, Jul. 2021.

[29] P. Gong, Z. Yan, W. Zhang, and J. Tang, "Trajectory tracking control for autonomous underwater vehicles based on dual closed-loop of mpc with uncertain dynamics," *Ocean Engineering*, vol. 265, DOI https://doi.org/10.1016/j.oceaneng.2022.112697, p. 112697, 2022. [Online]. Available: https://www.sciencedirect.com/science/article/pii/S0029801822019801

[30] Y. Zhang, C. Edwards, M. Belmont, and G. Li, "Robust model predictive control for constrained linear system based on a sliding mode disturbance observer," *Automatica*, vol. 154, DOI https://doi.org/10.1016/j.automatica.2023.111101, p. 111101, 2023. [Online]. Available: https://www.sciencedirect.com/science/article/pii/S0005109823002613

[31] H. Blom and Y. Bar-Shalom, "The interacting multiple model algorithm for systems with markovian switching coefficients," *IEEE Transactions on Automatic Control*, vol. 33, DOI 10.1109/9.1299, no. 8, pp. 780–783, 1988.

[32] C. Shen, Y. Shi, and B. Buckham, "Trajectory tracking control of an autonomous underwater vehicle using lyapunov-based model predictive control," *IEEE Transactions on Industrial Electronics*, vol. 65, DOI 10.1109/tie.2017.2779442, no. 7, pp. 5796–5805, Jul. 2018.

[33] J. Deshpande, T. Upadhyay, and D. Lainiotis, "Adaptive control of linear stochastic systems," *Automatica*, vol. 9, DOI 10.1016/0005-1098(73)90017-4, no. 1, pp. 107–115, Jan. 1973.

[34] Y. Shi, C. Shen, H. Wei, and K. Zhang, *Advanced Model Predictive Control for Autonomous Marine Vehicles.* Springer International Publishing, 2023.

[35] A. Robust, P. Control, A. for, U. Robotic, and Vehicles, "A robust predictive control approach for underwater robotic vehicles," *IEEE Transactions on Control Systems Technology*, vol. 28, DOI 10.1109/tcst.2019.2939248, no. 6, pp. 2352–2363, Nov. 2020.

[36] A. Nikou, C. K. Verginis, S. Heshmati-alamdari, and D. V. Dimarogonas, "A robust non-linear mpc framework for control of underwater vehicle manipulator systems under high-level tasks," *IET Control Theory & Applications*, vol. 15, DOI 10.1049/cth2.12045, no. 3, pp. 323–337, Dec. 2020.

[37] S. J. Julier and J. K. Uhlmann, "Unscented filtering and nonlinear estimation," *Proc. IEEE*, vol. 92, DOI 10.1109/jproc.2003.823141, no. 3, pp. 401–422, Mar. 2004.

[38] A. Jazwinski, *Stochastic Processes and Filtering Theory*, ser. Dover Books on Electrical Engineering Series. Dover Publications, 2007. [Online]. Available: https://books.google.co.jp/books?id=4AqL3vE2J-sC

[39] D. Simon, *Optimal State Estimation: Kalman, H∞, and Nonlinear Approaches*. Hoboken, NJ, USA: Wiley, Jan. 2006.

[40] G. Ackerson and K. Fu, "On state estimation in switching environments," *IEEE Transactions on Automatic Control*, vol. 15, DOI 10.1109/tac.1970.1099359, no. 1, pp. 10–17, Feb. 1970.

[41] Y. Bar-Shalom, X. Li, and T. Kirubarajan, *Estimation with Applications to Tracking and Navigation: Theory, Algorithms and Software*. New York, NY, USA: Wiley, Jan. 2002.

[42] X. R. Li and V. Jilkov, "Survey of maneuvering target tracking. part v: multiple-model methods," *IEEE Transactions on Aerospace and Electronic Systems*, vol. 41, DOI 10.1109/taes.2005.1561886, no. 4, pp. 1255–1321, Oct. 2005.

[43] B. Ristic, S. Arulampalam, and N. Gordon, *Beyond the Kalman Filter: Particle Filters for Tracking Applications*. Artech House, 2003. [Online]. Available: https://books.google.co.jp/books?id=zABIY--qk2AC

[44] D. G. LAINIOTIS, J. G. DESHPANDE, and T. N. UPADHYAY, "Optimal adaptive control: A non-linear separation theorem†," *International Journal of Control*, vol. 15, DOI 10.1080/00207177208932202, no. 5, pp. 877–888, May. 1972. [Online]. Available: http://www.tandfonline.com/doi/abs/10.1080/00207177208932202

[45] D. G. Lainiotis, "Partitioned estimation algorithms, i: Nonlinear estimation," *Information Sciences*, vol. 7, DOI 10.1016/0020-0255(74)90015-2, pp. 203–235, Jan. 1974.

[46] A. Antoniou and W.-S. Lu, *Practical Optimization: Algorithms and Engineering Applications*. Springer US, 2021.